Theoretical and Applied Climatology (2021) 143:901–913
https://doi.org/10.1007/s00704-020-03461-4

ORIGINAL PAPER

Tropical Atlantic dust and the zonal circulation

Mark R. Jury[1,2] · Angelie T. Nieves Jiménez[2]

Received: 26 April 2020 / Accepted: 9 November 2020 / Published online: 16 November 2020

Abstract

This study examines the factors driving the variability of Saharan dust over the subtropical Atlantic during summer. Monthly tropospheric dust concentrations from satellite-based model assimilation averaged in the area 10–23 N, 30–65 W, are used to create an index over the period 1980–2017. The seasonal cycle peaks in summer and affects tropical cyclones from July to September. Point-to-field regression analysis is performed, and then composites of dusty and clean seasons are analyzed as maps and sections of meteorological fields. The regression reveals significant differences in oceanic trade winds, (detrended) sea surface temperature, and atmospheric convection. Dusty minus clean composites show a zonal overturning circulation with sinking/rising motions over Africa/western Caribbean and lower easterlies/upper westerlies over the subtropical Atlantic. This circulation spreads Saharan dust and warm dry air in the 1–4 km layer westward at ~ 10 m/s over cooler waters, inhibiting convection. Among the factors driving tropospheric dust variability is the Pacific El Niño Southern Oscillation. Composites of dusty and clean hurricane occurrence show a threefold difference in numbers and a tenfold difference in mean power dissipation index. Analysis of a dust event in August 2009 illustrates how wind shear and cool SST conspire to suppress tropical easterly waves. Supplementary work characterizes the dispersion of a dense Saharan dust plume in June 2020.

1 Introduction

Every summer (Jun–Aug) dust plumes from the Sahara Desert are transported across the Atlantic Ocean by the prevailing winds (Engelstaedter and Washington 2007; Jury 2018). Annual dust emissions vary from 400 to 2200 Tg yr^{-1} (Huneeus et al. 2011) and have characteristic particle sizes < 50 μm (Van der Does et al. 2016). The dust forms a layer 1–4 km deep over the northeast Atlantic and displays multi-year variability (Prospero and Mayol-Bracero 2013).

The Sahara Desert is the largest mineral dust source providing about 50% of global emissions (Prospero et al. 2002). Dust plumes often precede or follow African easterly waves (AEW) that pass across the Sahel from July to September (Jones et al. 2003; Barkan et al. 2004; Washington and Todd 2005; Knippertz and Todd 2010; Huang et al. 2010). The dust-laden air is transported into the Atlantic by anticyclonic eddies within low level easterly winds (Karyampudi and Carlson 1988; Klose et al. 2010), passing over a cool marine layer capped by an inversion near 2 km elevation. Cuesta et al. (2009) describe the processes involved in the dispersion of dust plumes over west Africa: diurnal mixing, topographic effects, and transient wind events. Senghor et al. (2017) highlight structural changes in dust plumes entering the east Atlantic via the summer-time African easterly jet. Clean northerly marine flow undercuts the terrestrial air mass; the westward-moving dust plume is drawn into the 2–4 km layer due to anticyclonic subsidence over upwelled waters. The dry dusty Saharan air layer tends to suppress summer rainfall in the Caribbean (Mote et al. 2017, their Fig. 8c).

Aerosols absorb and scatter radiation selectively, making the dust layer warmer than the surrounding air (Petzold et al. 2011) and reducing net solar radiation to the underlying ocean (Jury and Whitehall 2010). Although dust aerosols may serve as cloud condensation nuclei, the presence of hot dry Saharan air overlying ocean upwelling inhibits the development of AEW that emerge from the coast (Dunion and Velden 2004; Wong et al. 2009; Jury and Santiago 2010). Dusty years tend to precede warm-phase Pacific El Niño Southern Oscillation (ENSO) conditions over the Sonoran Desert (Okin and Reheis 2002). Although Atlantic hurricanes respond to ENSO-modulated winds and SST (Nolan and McGauley 2012), and ENSO altered dust concentrations have been reported for the northwest Indian Ocean (Banerjee and Kumar 2016), similar links have not been reported for the tropical Atlantic.

✉ Mark R. Jury
mark.jury@upr.edu

[1] University of Zululand, Kwadlangezwa 3886, South Africa

[2] University of Puerto Rico Mayagüez, Mayagüez, PR 00681, USA

Table 1 Ranking of July–September tropospheric AOD 1980–2017 and concurrent hurricane power dissipation index (PDI) $\times 10^6$ m^3/s^2 in the tropical Atlantic

Dusty	JAS		Clean	JAS	
tropAOD	PDI	years	tropAOD	PDI	years
0.229	599	1981	0.165	2474	1996
0.334	138	1982	0.158	500	1997
0.257	0	1983	0.154	2039	1999
0.229	98	1984	0.167	120	2002
0.283	43	1991	0.144	3344	2004

During the hot summer months (June–August), Saharan dust is lifted into a ~ 5 km mixed layer (Gamo 1996; Garcia-Carreras et al. 2015; Jury 2018) and advected westward over the Atlantic. After particle deposition, a plume of fine dust reaches the Caribbean (Doherty et al. 2006; Reed et al. 2019; Jury 2017; Senghor et al. 2017).

Our main objective is to characterize the meteorological conditions associated with above and below normal occurrence of dust plumes passing from the Saharan desert across the tropical Atlantic to the Caribbean. Secondary objectives are to relate summer-time variations in east Caribbean dust concentrations with regional climate drivers and local hurricane frequency and intensity. We also briefly consider the rate of transport and dispersion in leading dust plume events.

2 Data and methods

Satellites that estimate dust aerosol concentrations represented by aerosol optical depth (AOD) typically measure the scattering of ultraviolet light by fine aerosols and include the Total Ozone Mapping Spectrometer (TOMS), Stratospheric Aerosol and Gas Measurements (SAGE), Moderate Resolution Imaging Spectrometer (MODIS), Optical Spectrograph and InfraRed Imaging System (OSIRIS), Global Ozone Monitoring by Occultation of Stars (GOMOS), Ozone Monitoring Instrument (OMI), and the Multi-angle Imaging SpectroRadiometer (MISR). Dust aerosol concentrations are estimated by sun photometers of the Aerosol Robotic Network (AERONET) and by the Micro-Pulse Lidar Network and help calibrate the satellite radiometers after screening for cloud effects. Drame et al. (2015) determined that Saharan dust aerosols at Dakar have a 1–8 μm diameter and can reduce solar transmittance by 70% for AOD values ~ 1. Numerical data assimilation combines the in situ and satellite data with emission inventories to produce dust concentration estimates over the period 1980–2017. Two such reanalysis products are MERRA-2 GEOS-5 (Molod et al. 2015; Randles et al. 2017; Buchard et al. 2017) and Global Aerosol Climatology Project (GACP; Geogdzhayev et al. 2005), the former having sub-daily time resolution and 60 km horizontal resolution. Average dust profiles over the tropical Atlantic are calculated from Cloud-Aerosol Lidar and Infrared Pathfinder Satellite Observations (CALIPSO) at 0.1 km vertical resolution.

An AOD index is obtained by averaging monthly MERRA2 and GACP AOD values over the Atlantic area, 10–23 N, 30–65 W, and then subtracting the global stratospheric component (Ridley et al. 2014; Vernier et al. 2011). This is hereafter referred to as the tropospheric AOD index and provides the basis for statistical study. In addition, we analyze two NOAA satellite products, sea surface temperature (SST) and net outgoing longwave radiation (OLR), as a proxy for moist convection. The NCEP2 reanalysis (Kanamitsu et al. 2002) offers monthly temperature, humidity, and wind circulation fields to analyze the meteorological context for aerosols over the tropical northeast Atlantic. The SODA3 ocean reanalysis is used to describe subsurface sea temperatures across the tropical Atlantic (Carton et al. 2018). All sea temperature data were detrended to remove multi-decadal influence (Vimont and Kossin 2007).

Dust plumes are most frequent in July, but local hurricane impacts include the following 2 months. The tropospheric AOD index shown in Fig. 2a is used to calculate linear point-to-field correlation maps in the July–September period 1980–2017 with respect to 850 hPa zonal wind and detrended SST. Statistical significance above 90% confidence is achieved with a correlation above $|0.29|$ for 38 degrees of freedom.

Based on a ranking of the July–September tropospheric AOD index, five high and low seasons were determined for composite analysis. The dusty years include 1981, 1982, 1983, 1984, and 1991; and the clean years include 1996, 1997, 1999, 2002, and 2004 (cf. Table 1). Composites were formed by subtracting the clean Jul–Sep seasons from the dusty seasons for the following fields: relative humidity, upper and surface winds, air and sea temperature, and net OLR. Hurricane tracks and intensities from the official NOAA database were analyzed for dusty vs clean seasons. The Jul–Sep power dissipation index (PDI, Emanuel 2005) is obtained as a measure of intensity, defined as the sum of maximum 1-min sustained wind speed cubed, at 6-h intervals, for all periods when the cyclone is at least tropical storm category within the index area. Our statistical analysis makes use of the Southern Oscillation Index (SOI) extracted from NOAA CPC as the standardized pressure difference between Darwin and Tahiti, and zonal wind shear calculated as 200 hPa minus 850 hPa U component, where + refers to westerly shear.

The summer with highest AOD in the recent decade (2009) is analyzed for aerosol and meteorological conditions using cMorph multi-satellite rainfall (Joyce et al. 2004), NOAA SST fields, MERRA2 tropospheric AOD, MERRA2 low level

winds, potential vorticity, and convective inhibition, calculated as the vertically integrated departure from moist adiabatic lapse rate. During the period 21–24 August 2009 when a dust plume surrounded a tropical easterly wave over the Atlantic, we analyze radiosonde profiles and vertical sections on 30 W of CALIPSO aerosol density, MERRA2 ozone concentration, and the meridional circulation. This case study and another in the supplementary section employ more recent satellite technology for detection of vertical structure <https://www.wmo-sat.info/oscar/gapanalyses?variable=6>.

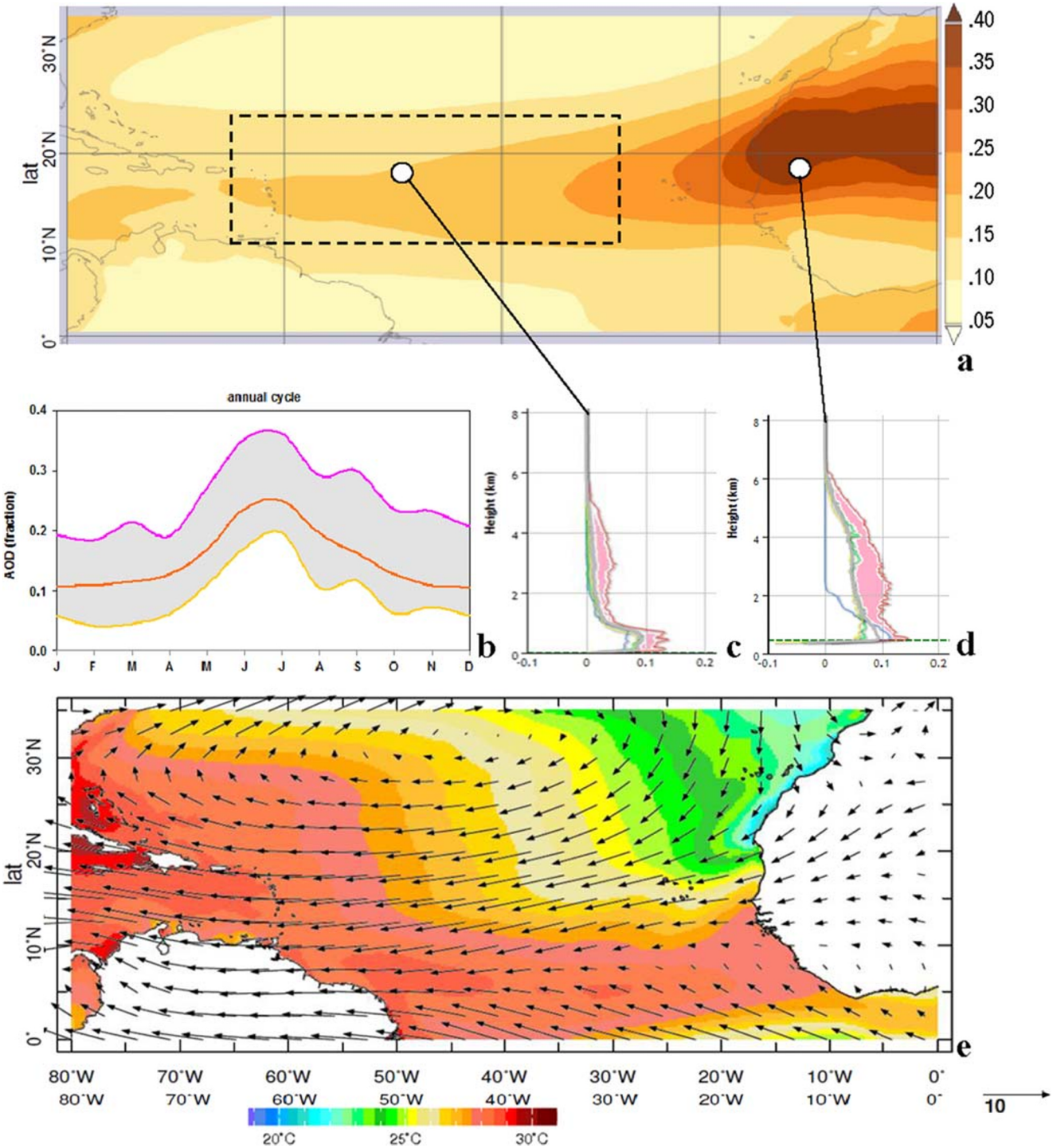

Fig. 1 (**a**) MERRA2 aerosol optical depth (fraction) June–August 1980–2017, with shaded plume and dashed index area: 10–23 N, 30–65 W. (**b**) Mean annual cycle of tropospheric AOD over the tropical Atlantic index area, with upper and lower quintiles. Mean vertical profiles of seasonal CALIPSO aerosol density: (**c**) 19 N, 50 W and (**d**) 19 N, 10 W (positions denoted); with winter-blue, spring-green, summer-pink, autumn-yellow. Climatology maps of 1980–2017 Jun–Aug mean: (**e**) NOAA SST and MERRA2 925–700 hPa wind vectors

A forward particle trajectory analysis of the Aug 2009 event is conducted using the Hysplit dispersion algorithm (Stein et al. 2015). Dust concentrations and transport are studied by Hovmoller analysis of MERRA2 tropospheric AOD averaged 10–23 N from 80 to 0 W, to show contrasts between a clean spell 1–20 Aug 2015 (with AOD < 0.1) and the dusty case of 10–30 Aug 2009. Scatterplots of monthly tropospheric AOD vs zonal wind shear and detrended SST in the tropical Atlantic are segregated by Pacific Southern Oscillation Index (SOI), to further our statistical insights. Lastly a supplementary analysis is made of an extreme dust event in June 2020 using model, satellite, and station datasets.

3 Results

3.1 Seasonal conditions and correlation maps

Mean summer aerosol concentrations illustrate a dust plume emerging from West Africa with a tropospheric AOD fraction > 0.4 (Fig. 1a). The dust is transported above a marine layer (cf. Senghor et al. 2017, their Fig. 5c) as it disperses westward across the tropical Atlantic, reaching the eastern Caribbean with an AOD value of 0.2. The annual cycle of tropospheric AOD within the index area peaks in early summer (Fig. 1b). AOD begins to rise in April from 0.10 to 0.25 and decreases gradually after September. The main axis of the dust plume is

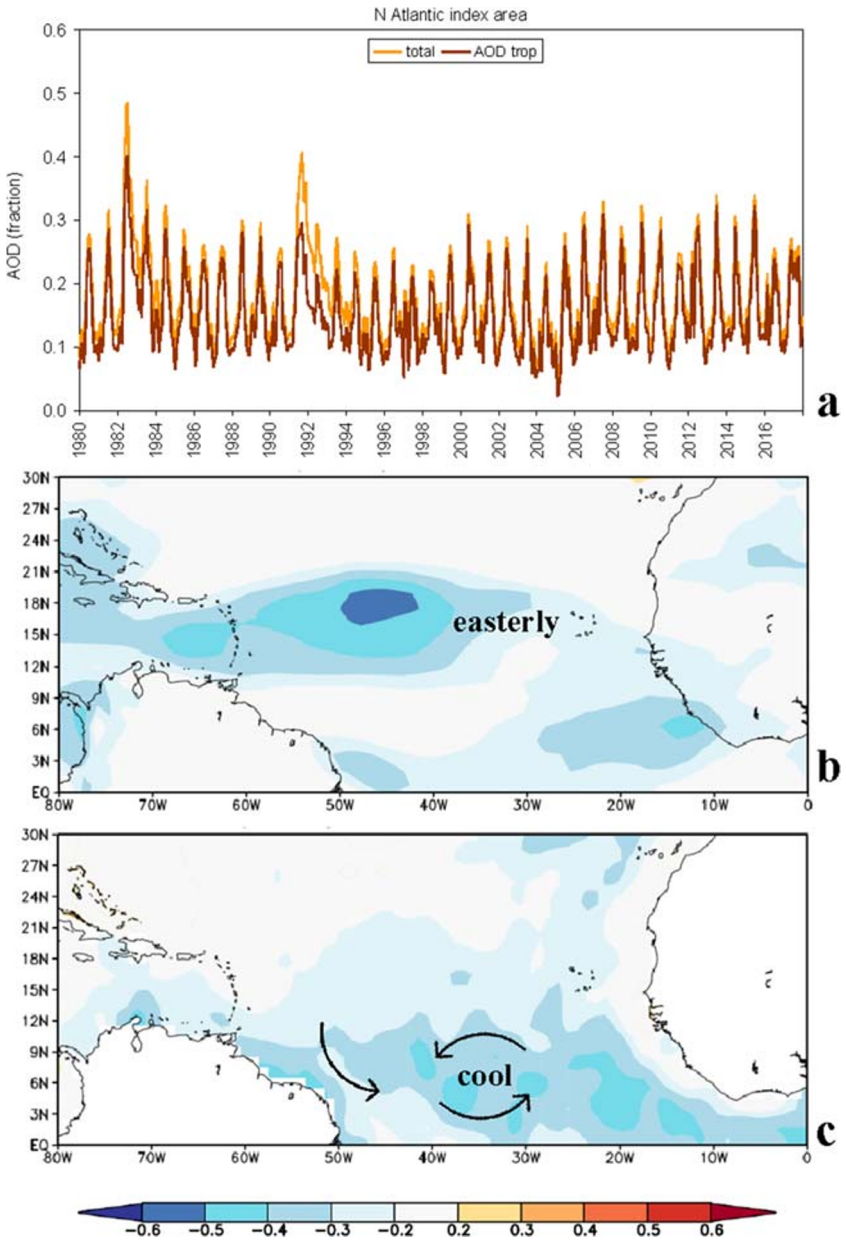

Fig. 2 (**a**) North tropical Atlantic index area total and tropospheric AOD time series. Correlation of Jul–Sep tropospheric AOD values 1980–2017 with fields of (**b**) MERRA2 850 hPa zonal wind and (**c**) detrended NOAA SST and schematic currents in the equatorial Atlantic. Correlations − 0.2 to 0.2 are unshaded

along 20 N, in alignment by transport from the Saharan source region. The dust plume is > 4 km deep over West Africa and undergoes gradual deposition along its 3000 km path toward the Caribbean. The mean CALIPSO profiles over the northeast Atlantic in Fig. 1 c and d indicate a thinning of the dust layer to 1 km depth (Doherty et al. 2006, 2012). Vertical confinement is attributed to an inversion over the Canary upwelling plume (SST < 25C) that continues downwind under subsidence caused by trade wind divergence (Fig. 1e). Highest CALIPSO dust concentrations over the index area occur within the marine boundary layer, which is smoothed in MERRA2 reanalysis (Buchard et al. 2017, their Fig. 2).

Figure 2a shows the monthly AOD time series over the index area since 1980 and reflects seasonal spikes during summer and following two significant volcanic eruptions (4 Apr 1982, 15 Jun 1991) which coincided with the onset of Pacific El Niño. With the stratospheric contribution subtracted, the highest seasonal tropospheric AOD fraction was in 1982 (0.334), while the lowest value over the tropical Atlantic was in 2004 (0.144; cf. Table 1). The tropospheric AOD index has a weak downtrend arising from dust events in the 1980s and increased Sahel rainfall thereafter (Foltz and McPhaden 2008; Evan et al. 2016). Figure 2b shows the Jul–Sep point-to-field correlation of the tropospheric AOD index and 850 hPa zonal wind. Values < − 0.5 in the tropical Atlantic Ocean indicate the coincidence of near-surface easterly flow and higher dust concentration, as expected. The easterly winds also induce local evaporative cooling of the sea surface. Hence the Jul–Sep AOD correlation with detrended SST reveals negative values (Fig. 2c) beneath the dust plume and also in the tropical zone (5–10 N) due to the cyclonic rotation of currents, wind stress curl, and consequent upwelling, a well-known oceanographic process (Smith 1968; Bakun and Nelson 1991). The transport of Saharan dust to the Caribbean coincides with strengthened anticyclonic trade winds and cooler SSTs across the tropical Atlantic.

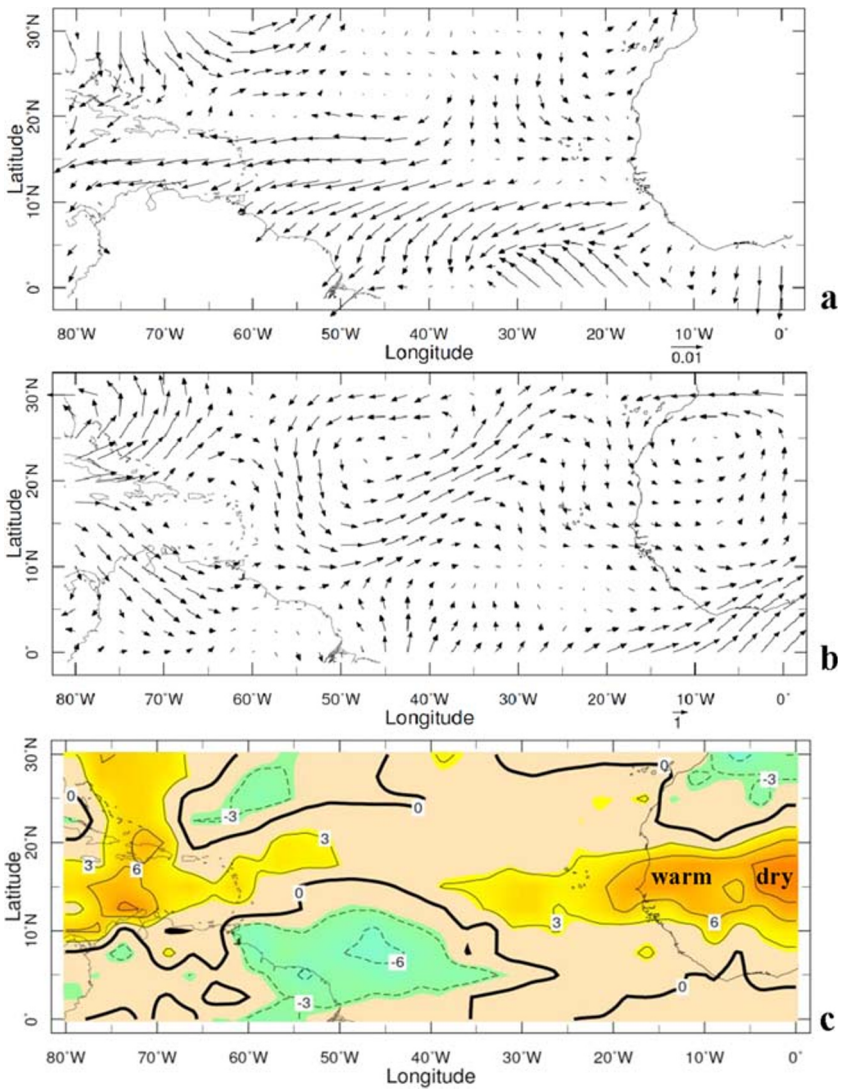

Fig. 3 Dusty minus clean Jul–Sep composites of (**a**) surface wind stress (N/m^2), (**b**) 200–250 hPa winds (m/s), and (**c**) satellite net OLR (W/m^2) differences

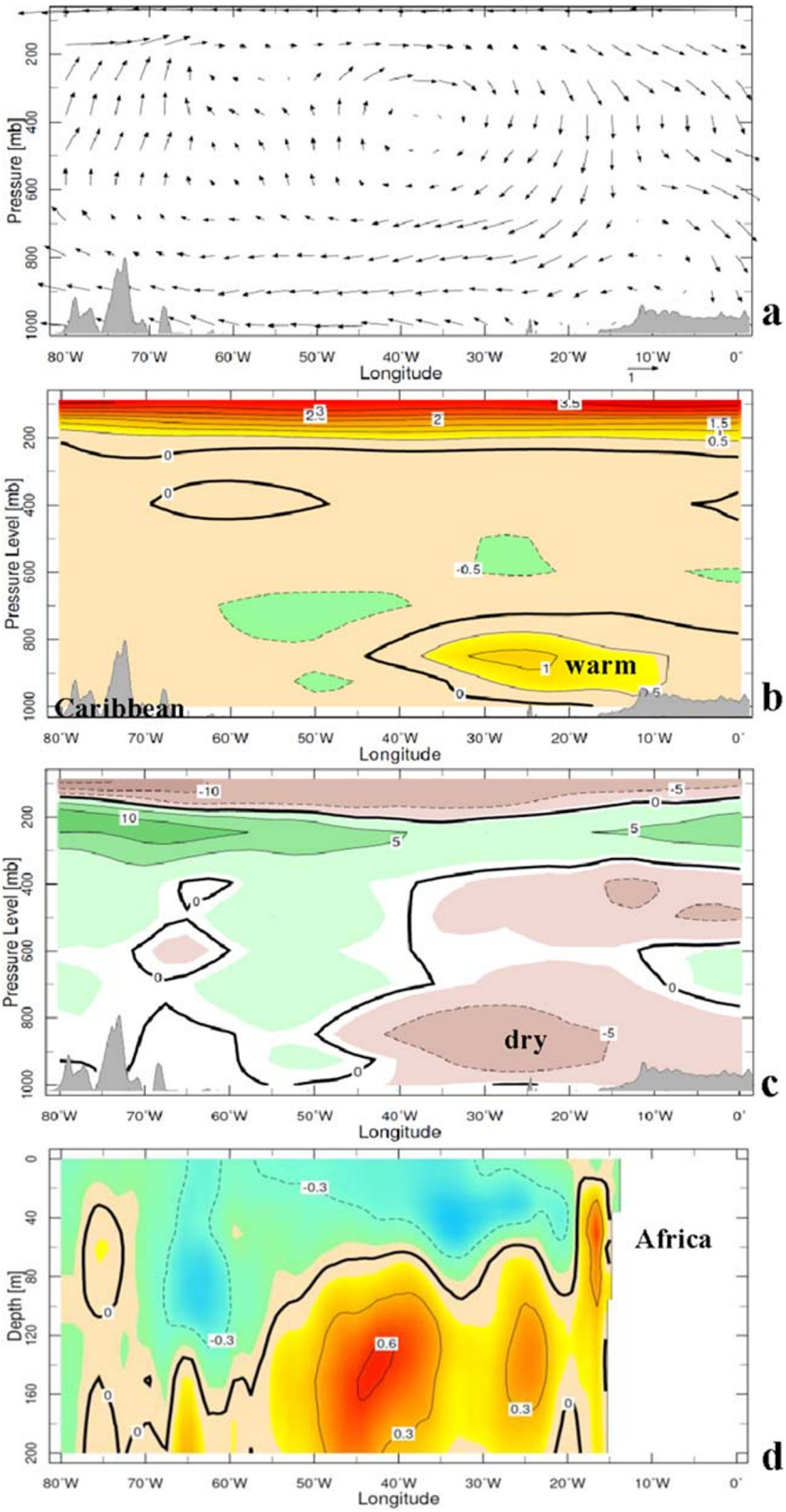

Fig. 4 West-east vertical sections averaged 10–23 N of composite dusty minus clean Jul–Sep: (**a**) NCEP2 zonal atmospheric circulation (m/s, U + W components), (**b**) air temperature (°C), (c) specific humidity (g/kg), and (**d**) SODA3 detrended subsurface sea temperature (°C); all represent differences. (**a**) illustrates a coherent Walker circulation

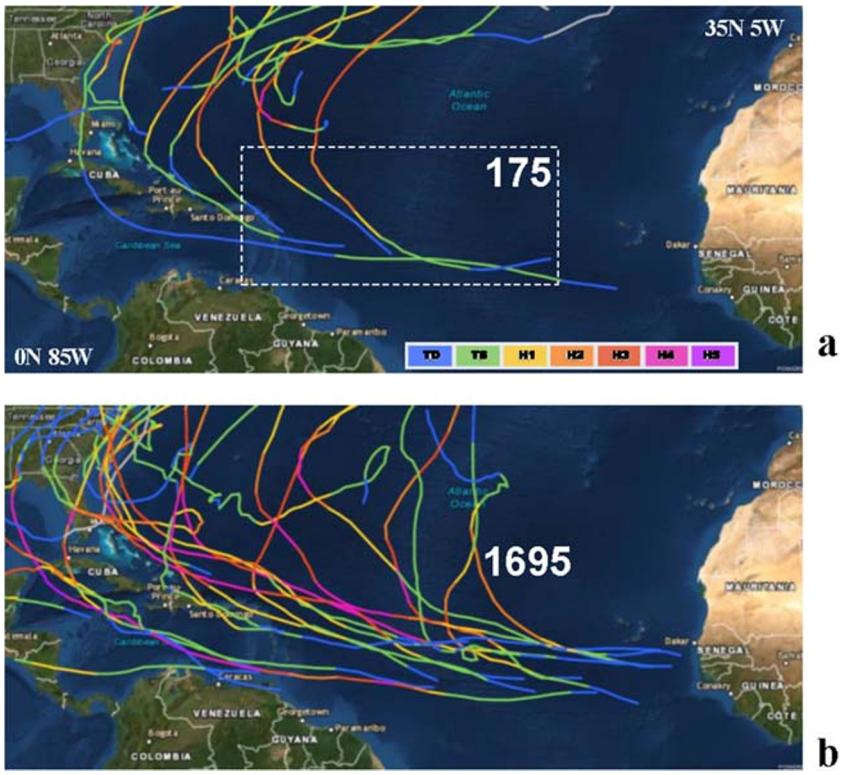

Fig. 5 Hurricane tracks during (**a**) dusty seasons and (**b**) clean seasons, based on Table 1. Large white numbers are mean PDI value in the index area (dashed); colors represent tropical cyclone intensity according to SS scale (upper)

3.2 Composite climate and ocean

Composite results were derived from the ranking of index area tropospheric AOD (Table 1). The average of dusty years has an AOD fraction 0.11 above clean years, with max and min years: 1982 and 2004. Dusty years show a wider range than clean years. The Jul–Sep index area PDI is listed and reveals an increased frequency of stronger tropical cyclones in "clean" years (1695 vs 175 10^6 m^3/s^2), albeit with outliers in each category from multivariate influences (Evan et al. 2006). The dusty minus clean composite of winds (Fig. 3a, b) show an increase of both surface easterly flow and upper westerly flow. Surface southeasterly winds expand across the equator in 15–30 W longitudes, inducing upwelling and lower SST there (cf. Fig. 2c). Thus air-sea interactions are stronger on the equatorial flank of the dust plume, e.g., large vector differences in Fig. 3b along 5 N from 25 to 40 W, and inhibit local thermodynamic energy. In the zone 12–20 N, the net OLR differences > + 5 W/m^2 (Fig. 3c) indicate reduced cloudiness. That axis of subsidence extends from West Africa to the Caribbean and refers to fewer and weaker tropical easterly waves in dusty years (Jury and Santiago 2010).

Composite circulation differences between dusty and clean years are shown in vertical perspective in Fig. 4a. The overturning lower easterly and upper westerly winds form a conveyor belt of rising motion over the western Caribbean (75 W) and sinking over Africa (15 W). This anomalous Walker circulation is a remarkably coherent feature that unites our inferences on enhanced dust generation, westward transport, regional climate, air-sea interaction, and local weather impacts, as seen below.

Air temperatures and specific humidity differences in the plume emerging from Africa are warm (+ 1.0C) and dry (− 5 g/kg) (Fig. 4b, c). Accompanying the near-surface features, the tropopause is warmer in dusty summers. Sea temperature differences reflect cooler conditions (− 0.3C) in a layer that deepens from 60 m at 30 W to 120 m at 65 W (Fig. 4d) under intensified trade winds. This stable condition inhibits cloud convection and suppresses tropical easterly waves. Sea temperature differences of that

Table 2 Southern oscillation correlation at various lags with the July–September tropical Atlantic tropospheric AOD index over the period 1980–2017 (− = before). *p* value basis is 38 degrees of freedom

Months	Lag	Corr	*p* val
AMJ	− 3	−0.012	0.946
MJJ	− 2	−0.103	0.587
JJA	− 1	−0.110	0.552
JAS	0	−0.126	0.498
ASO	1	−0.138	0.461
SON	2	−0.200	0.279
OND	3	−0.259	0.153
NDJ	4	−0.321	0.081
DJF	5	−0.301	0.094
JFM	6	−0.296	0.096

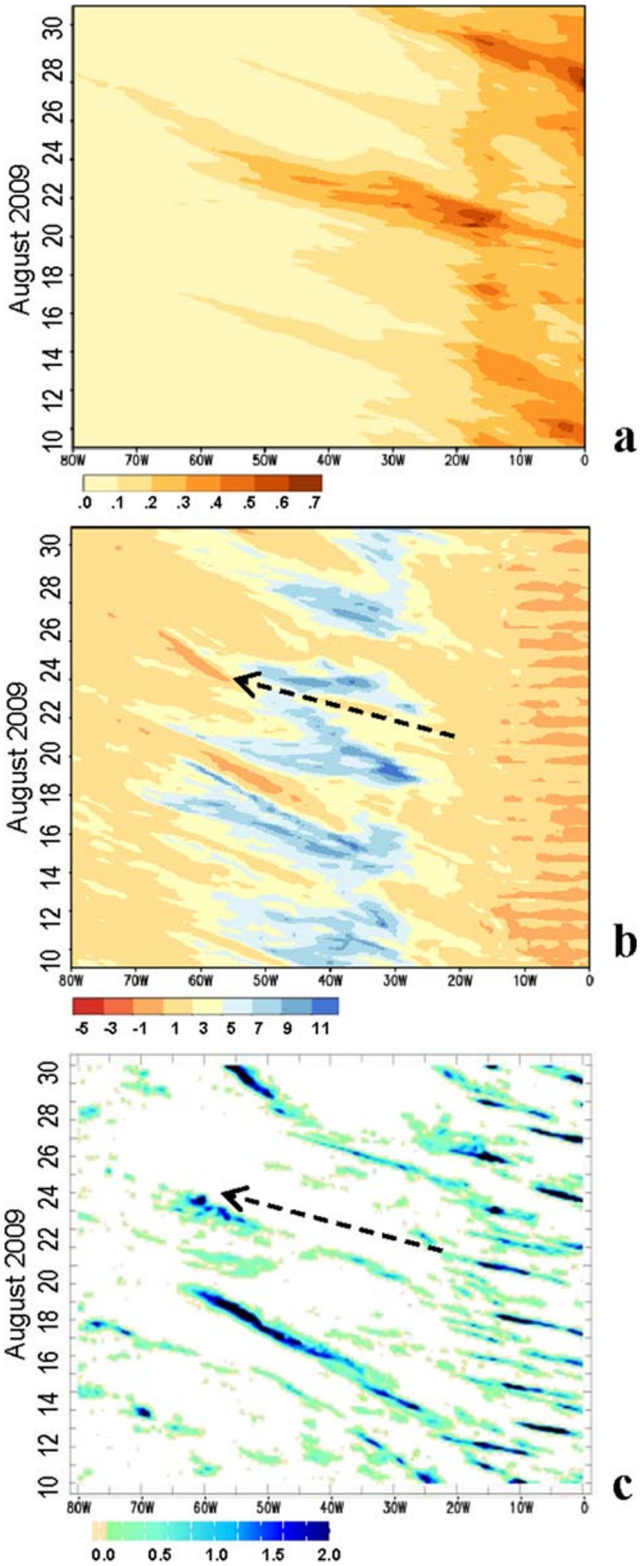

Fig. 6 Hovmoller analysis August 2009 averaged 10–23 N of (**a**) MERRA2 tropospheric AOD fraction, (b) MERRA2 850 hPa potential vorticity (10^{-7} s^{-1}), and (**c**) cMorph satellite rainfall (mm/h). All have 3-h resolution. The dashed arrow refers to dust transport during the event of ~ 11 m/s

depth are beyond the reach of surface forcing and suggest modulation by Atlantic Ocean Rossby waves (Chu et al. 2007; Ding et al. 2009).

3.3 Hurricanes, dust, and ENSO

Figure 5a and b compare Caribbean hurricane activity in dusty and clean seasons: 5 vs 16. The threefold increase is attributed to three conspiring features: (i) increased westerly wind shear, (ii) cooler SST, and (iii) more dust over the tropical Atlantic (cf. Figs. 2c and 4a), among other factors (Goldenberg et al. 2001).

Table 2 lists the correlation between Jul–Sep index area AOD and Pacific SOI at various lags. Months + 3 to + 6 (following winter) show negative correlation values that reach 90% confidence. We infer that Pacific ENSO phase modulates the Atlantic zonal circulation which advects Saharan dust (cf. Fig. 4a). African easterly waves emerging from the Sahel must contend with subsidence, westerly shear, and reduced SST; all united by the anomalous Walker circulation and its consequences.

3.4 Case study 2009

The most recent dusty summer in our group (2009) is analyzed in Figs. 6, 7 and 8 to quantify event-scale dispersion. Easterly winds over the Sahara advected dust plumes in June and July and also in the period 21–24 August, our focus here. Hovmoller analysis of MERRA2 AOD (Fig. 6a) exhibited westward transport of a dust plume from 20 W to 55 W over the 4-day period (~ 10 m/s).

Diagonal bands of 850 hPa cyclonic vorticity and rainfall in the dusty spell (Aug 2009) coincide in the Hovmoller analysis 10–23 N (Fig. 6b, c). Yet below the dust plume, anticyclonic vorticity and dry conditions were noted, as in Zuluaga et al. (2012, their Fig. 5). Maps averaged 23–24 August (Fig. 7a–c) show a Saharan dust plume meandering toward the Caribbean over a zone of cool SST < 26C with convective inhibition < − 300 J/kg. Low level winds and satellite rainfall show undulating easterly flow and convection associated with AEW at 55 W and 15 W, the latter embedded in the dust plume. Radiosonde profiles (Fig. 8a) indicate stable conditions over West Africa and the adjacent Atlantic with convective inhibition < − 1000 J/kg at Tenerife and 700–600 hPa easterly winds > 20 m/s at Dakar. CALIPSO vertical sections (Fig. 8b, c) illustrate a dust plume extending from 12 to 27 N in a 3–6 km layer over the tropical east Atlantic 30–38 W.

The vertical section on 30 W of MERRA2 ozone concentration and meridional circulation during the case study offers a unique perspective in Fig. 8d. Within the convective area (10 N), meridional convergence lifts low ozone marine air (< 60 ppb) in a narrow tower that is confined by subsidence around the edges

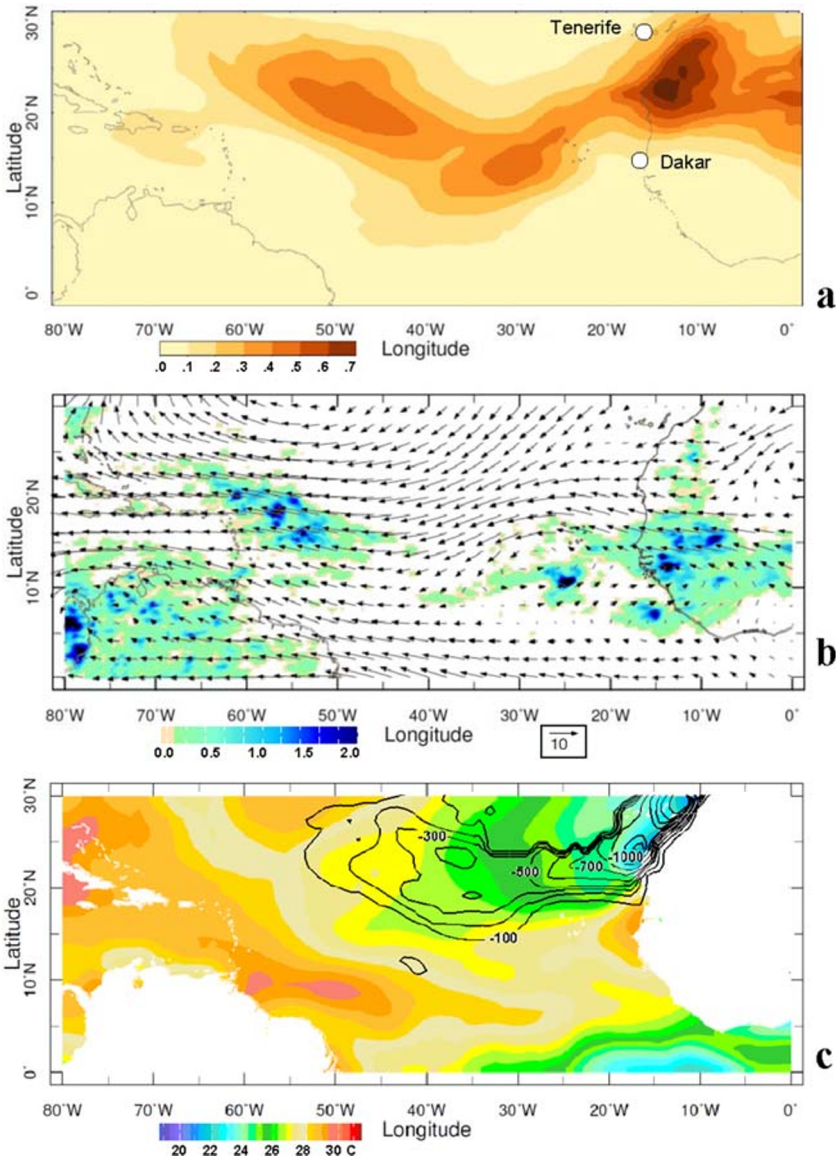

Fig. 7 Case study maps 23–24 August 2009: (**a**) MERRA2 tropospheric AOD dust plume, (**b**) 925–700 hPa wind vectors and cMorph rainfall (shaded, mm/h), and (**c**) SST field and convective inhibition (contour < − 100 J/kg). Dots in (**a**) show radiosonde profiles in Fig. 8

characterized by high ozone air (> 100 ppb). A Hysplit forward particle trajectory analysis (Fig. 8e) suggests that the dust plume spreads west of Africa at ~ 12 m/s over the period 21–23 August 2009, along the northern edge of a convective wave. The Hysplit-simulated plume disperses above the marine layer consistent with the CALIPSO sections (cf. Fig. 8b, c).

To improve understanding, we present a contrasting clean spell in early August 2015 (Fig. 9a) that reveals an absence of dust in Caribbean longitudes (AOD < 0.2) consistent with slower transport (~ 4 m/s) west of Africa. This points to a lull in the African easterly jet that carries both tropical waves and sub-tropical dust. Buchard et al. (2017) provide a Saharan dust plume analysis in their section 4b and conclude that the MERRA2 reanalysis faithfully represents transport and dispersion to the Caribbean in comparison with in situ and satellite measurements.

4 Discussion

Our research has quantified dust transport over the tropical Atlantic in the period 1980–2017 via MERRA2 reanalysis and ancillary datasets. Dispersion of the summer mean dust plume (cf. Fig. 1a, c) followed the pattern of Senghor et al. (2017): AOD declined by half from West Africa to the Caribbean. A tropospheric dust index in the eastern Caribbean (10–23 N, 30–65 W) was employed to determine dusty and clean Jul–Sep seasons. The easterly winds that transport the dust plume also cool the sea surface by evaporation and cyclonic upwelling, in contrast with Zuluaga et al. (2012, their Fig. 6). Our composite analysis (cf. Fig. 4a) reflects an Atlantic zonal overturning circulation that sinks over West Africa, enhancing dust emissions there. These features inhibit African easterly waves entering a cooler Atlantic under westerly wind shear.

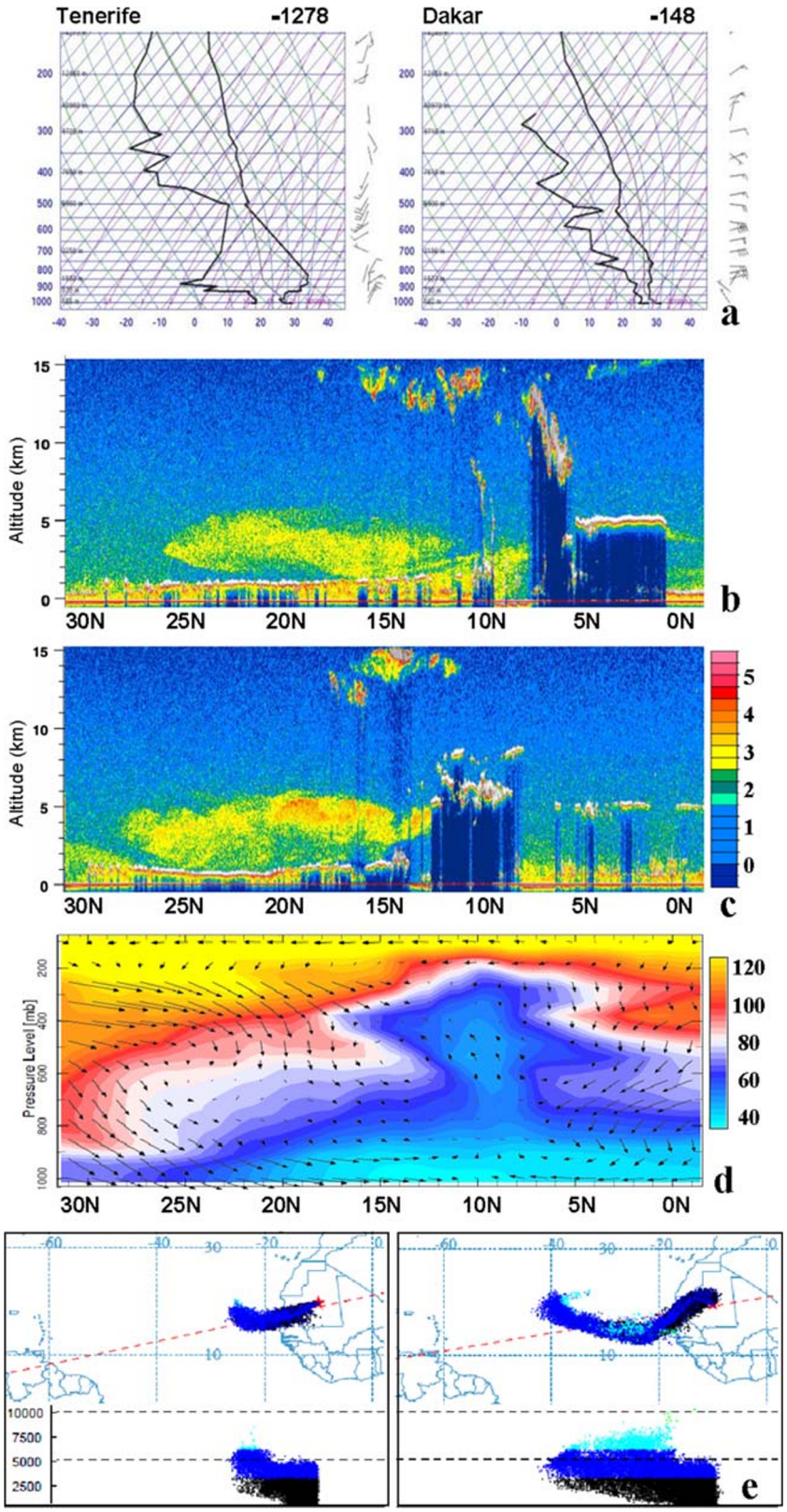

Fig. 8 (**a**) Case study radiosonde profiles (cf. Fig. 7a for stations) with convective inhibition listed (J/kg). CALIPSO vertical sections of aerosol backscatter 0.532 μm on (**b**) 20 Aug on 30 W and (**c**) 23 Aug 2009 on 38 W (10^{-3} sr^{-1} km^{-1}). (**d**) MERRA2 vertical section on 30 W of ozone concentration (ppb) and meridional circulation 22–24 Aug 2009. (**e**) Forward particle trajectories calculated by Hysplit for a continuous dust emission from 20 N, 10 W, 1000–3000 m layer, commencing 21 August 2009: after 24 (left) and 48 h, in map and section view (lower). The westward spread is > 12 m/s

Our research featured an anomalous Walker cell over the Atlantic (cf. Fig. 4a) that is associated with Pacific ENSO phase and consequential for Caribbean hurricanes. Figure 9b illustrates scatterplots of monthly index area tropospheric AOD versus zonal wind shear and detrended SST, segregated by SOI. The greater magnitude +/–SOI appear in the lower/

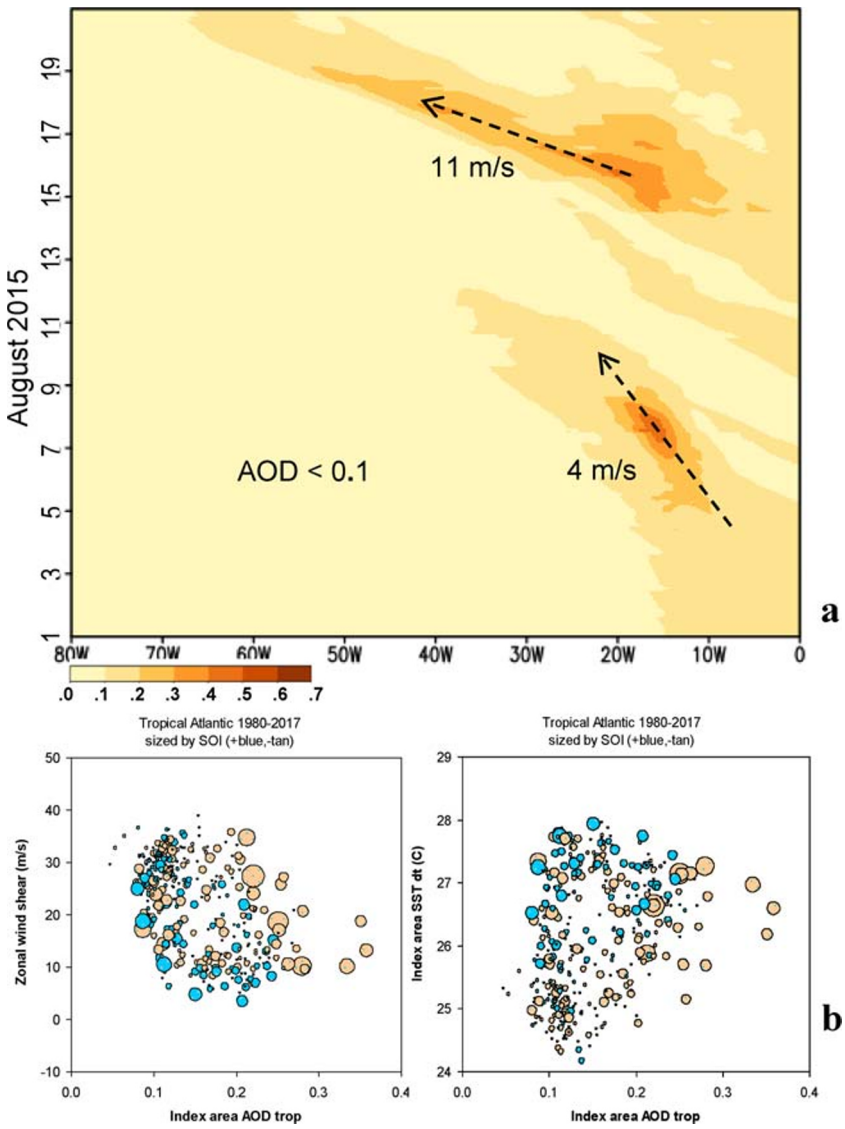

Fig. 9 (**a**) Hovmoller analysis averaged 10–23 N of MERRA2 tropospheric AOD during a "clean" spell 1–20 August 2015. Dashed lines refer to plume transport rates, for comparison with Fig. 6a. (**b**) Scatterplots of 1980–2017 monthly index area MERRA2 tropospheric AOD vs zonal wind shear (left) and detrended SST, with points sized by SOI +3 lag value and colored by sign (+blue −tan). Zonal wind shear = 200–850 U, + westerly

upper AOD across a range of zonal wind shear. We find a similar pattern for SST except the greater magnitude SOI cases tend to segregate above 27C. These underpin the notion that the Atlantic zonal overturning circulation induces easterly/westerly shear corresponding with warmer/cooler Atlantic SST prior to Pacific cool/warm phase. Although we have statistically segregated the Atlantic zonal circulation, sea temperatures, and dust concentrations, our composites suggest that these processes are united by a remarkably coherent Walker circulation (cf. Fig. 4a) and seldom act independently.

A case study in August 2009 highlighted key features: a dust plume extends westward from Africa to the Caribbean across latitudes 12–27 N and depths 2–5 km, overlying SST < 26C inducing convective inhibition < − 300 J/kg. The dust plume is accompanied by anticyclonic vorticity (cf. Fig. 6b) and sinking motions; so passing AEW entrain stable air and tend to weaken downstream over the Caribbean. In dusty spells, transport was 12 m/s, whereas in clean spells, the carrying easterly flow declined to 4 m/s. Dispersion rates appear to be controlled by downstream deposition and lateral plume spread. On-going studies (cf. Supplementary) illustrate an extreme dust plume event in June 2020, while further work will analyze the intra-seasonal nature of dust–environment interactions.

Supplementary Information The online version contains supplementary material available at https://doi.org/10.1007/s00704-020-03461-4.

Authors' contribution The first author conceived the research and analyzed much of the data; the second author provided interpretations.

Funding The first author has ongoing support from the SA Dept of Education.

Compliance with ethical standards

Conflict of interest The authors declare that they have no conflict of interest.

References

Bakun A, Nelson CS (1991) The seasonal cycle of wind stress curl in subtropical eastern boundary current regions. J Phys Oceanogr 21: 1815–1834

Banerjee P, Kumar SP (2016) ENSO modulation of interannual variability of dust aerosols over the Northwest Indian Ocean. J Clim 29: 1287–1303

Barkan J, Kutiel H, Alpert P, Kishcha P (2004) Synoptics of dust intrusion days from the African continent into the Atlantic Ocean. J Geophys Res 109:D08201. https://doi.org/10.1029/2003JD004416

Buchard V, 10 coauthors (2017) The MERRA-2 aerosol reanalysis, 1980 onward. Part II: evaluation and case studies. J Climate 30:6851–6872

Carton JA, Chepurin GA, Chen L (2018) SODA3: a new ocean climate reanalysis. J Clim 31:6967–6983

Chu PC, Ivanov LM, Melnichenko OV, Wells NC (2007) On long baroclinic Rossby waves in the tropical North Atlantic observed from profiling floats. J Geophys Res 112:C05032. https://doi.org/10.1029/2006JC003698

Cuesta J, Marsham JH, Parker DJ, Flamant C (2009) Dynamical mechanisms controlling the vertical redistribution of dust and the thermodynamic structure of the West Saharan atmospheric boundary layer during summer. Atmos Sci Lett 10:34–42

Ding H, Keenlyside N, Latif M (2009) Seasonal cycle in the upper equatorial Atlantic Ocean. J Geophys Res 114:C09016. https://doi.org/10.1029/2009JC005418

Doherty OM, Riemer N, Hameed S (2012) Control of Saharan mineral dust transport to Barbados in winter by the Intertropical Convergence Zone over West Africa. J Geophys Res 117:D19117. https://doi.org/10.1029/2012JD017767

Doherty RM, Stevenson DS, Johnson CE, Collins WJ, Sanderson MG (2006) Tropospheric ozone and El Niño–southern oscillation: influence of atmospheric dynamics, biomass burning emissions, and future climate change. J Geophys Res 111:D19304. https://doi.org/10.1029/2005JD006849

Drame MS, Ceamanos X, Roujean JL, Boone A, Lafore JP, Carrer D, Geoffroy O (2015) On the importance of aerosol composition for estimating incoming solar radiation: focus on the western African stations of Dakar and Niamey during the dry season. Atmosphere 6: 1608–1632

Dunion JP, Velden CS (2004) The impact of the Saharan air layer on Atlantic tropical cyclone activity. Bull Am Meteorol Soc 85:353–365

Emanuel K (2005) Increasing destructiveness of tropical cyclones over the past 30 years. Nature 436:686–688

Engelstaedter S, Washington R (2007) Atmospheric controls on the annual cycle of North African dust. J Geophys Res 112:D03103. https://doi.org/10.1029/2006jd007195

Evan AT, Dunion J, Foley JA, Heidinger AK, Velden CS (2006) New evidence for a relationship between Atlantic tropical cyclone activity and African dust outbreaks. Geophys Res Lett 33:L19813. https://doi.org/10.1029/2006GL026408

Evan AT, Flamant C, Gaetani M, Guichard F (2016) The past, present and future of African dust. Nature 531:493–497

Foltz GR, McPhaden MJ (2008) Trends in Saharan dust and tropical Atlantic climate during 1980-2006. Geophys Res Lett 35:1–5

Gamo M (1996) Thickness of the dry convection and large-scale subsidence above deserts. Bound-Layer Meteorol 79:265–278

Garcia-Carreras L, Parker DJ, Marsham JH (2015) The turbulent structure and diurnal growth of the Saharan atmospheric boundary layer. J Atmos Sci 72:693–713

Geogdzhayev IV, Mishchenko MI, Terez EI, Terez GA, Gushchin GK (2005) Regional AVHRR-derived climatology of aerosol optical thickness and size. J Geophys Res 110:D23205. https://doi.org/10.1029/2005JD006170

Goldenberg SB, Landsea CW, Mestas-Nunez AM, Gray WM (2001) The recent increase in Atlantic hurricane activity: causes and implications. Science 293:474–479

Huang JF, Zhang CD, Prospero JM (2010) African dust outbreaks: a satellite perspective of temporal and spatial variability over the tropical Atlantic Ocean. J Geophys Res 115:D05202. https://doi.org/10.1029/2009JD012516

Huneeus N, 29 coauthors (2011) Global dust model intercomparison in AeroCom phase I. Atmos Chem Phys 11:7781–7816

Jones C, Mahowald N, Luo C (2003) The role of easterly waves on African desert dust transport. J Climate 16:3617–3628

Joyce RJ, Janowiak JE, Arkin PA, Xie PP (2004) cMorph: a method that produces global precipitation estimates from passive microwave and infrared data at high spatial and temporal resolution. J Hydrometeorol 5:487–503

Jury MR (2017) Caribbean air chemistry and dispersion conditions in the satellite era. Atmosphere 8:151. https://doi.org/10.3390/atmos8080151

Jury MR (2018) Climatic modulation of early summer dust emissions over West Africa. J Arid Environ 152:55–68

Jury MR, Santiago MJ (2010) Composite analysis of dust impacts on African easterly waves in the MODIS era. J Geophys Res 115: D16213. https://doi.org/10.1029/2009JD013612

Jury MR, Whitehall K (2010) Warming of an elevated layer over Africa. Clim Chang 99:229–245

Kanamitsu M, co-authors (2002) NCEP–DOE AMIP-II reanalysis (R-2). Bull Am Meteorol Soc 83:1631–1643

Karyampudi VM, Carlson TN (1988) Analysis and Numerical Simulations of the Saharan Air Layer and Its Effect on Easterly Wave Disturbances. J Atmos Sci 45(21):3102–3136

Klose M, Shao Y, Karremann MK, Fink AH (2010) Sahel dust zone and synoptic background. Geophys Res Lett 37:L09802. https://doi.org/10.1029/2010GL042816

Knippertz P, Todd MC (2010) The central west Saharan dust hot spot and its relation to African easterly waves and extratropical disturbances. J Geophys Res 115:D12117. https://doi.org/10.1029/2009JD012819

Molod A, Takacs L, Suarez M, Bacmeister J (2015) Development of the GEOS-5 atmospheric general circulation model: evolution from MERRA to MERRA2. Geosci Model Dev 8:1339–1356

Mote TL, Ramseyer CA, Miller PW (2017) The Saharan air layer as an early rainfall season suppressant in the eastern Caribbean: the 2015 Puerto Rico drought. J Geophys Res Atmos 122:10966–10982

Nolan DS, McGauley MG (2012) Tropical cyclogenesis in wind shear: climatological relationships and physical processes. In: Oouchi K, Fudeyasu H (eds) Cyclones: formation, triggers, and control. Nova Science Pub, Happauge, pp 1–34

Okin GS, Reheis MC (2002) An ENSO predictor of dust emission in the southwestern United States. Geophys Res Lett 29:1332. https://doi.org/10.1029/2001GL014494

Petzold A, Veira A, Mund S, Esselborn M, Kiemle C, Weinzierl B, Hamburger T, Ehret G, Liebke K, Kandler K (2011) Mixing of mineral dust with urban pollution aerosol over Dakar (Senegal): impact on dust physico-chemical and radiative properties. Tellus B 63:619–634

Prospero JM, Mayol-Bracero OL (2013) Understanding the transport and impact of African dust on the Caribbean basin. Bull Am Meteorol Soc 94:1329–1337

Prospero JM, Ginoux P, Torres O, Nicholson SE, Gill TE (2002) Environmental characterization of global sources of atmospheric soil dust identified with the Nimbus 7 total ozone mapping spectrometer absorbing aerosol product. Rev Geophys 40:1002. https://doi.org/10.1029/2000RG000095

Randles CA, Silva AM, Buchard V, Colarco PR, Darmenov A, Govindaraju R (2017) The MERRA-2 aerosol reanalysis, 1980

onward. Part I: system description and data assimilation evaluation. J Climate 30:6823–6850

Reed KA, Bacmeister JT, Huff JJA, Wu X, Bates SC, Rosenbloom NA (2019) Exploring the impact of dust on North Atlantic hurricanes in a high-resolution climate model. Geophys Res Letters 46:1105–1112

Reid JS, Kinney JE, Westphal DL, Holben BN, Welton EJ, Tsay S-C, Eleuterio DP, Campbell JR, Christopher SA, Colarco PR, Jonsson HH, Livingston JM, Maring HB, Meier ML, Pilewskie P, Prospero JM, Reid EA, Remer LA, Russell PB, Savoie DL, Smirnov A, Tanré D (2003) Analysis of measurements of Saharan dust by airborne and ground-based remote sensing methods during the Puerto Rico Dust Experiment. J Geophys Res 108(D19):8586. https://doi.org/10.1029/2002JD002493

Ridley DA, Solomon S, Barnes JE, Burlakov VD, Deshler T, Dolgii SI, Herber AB, Nagai T, Neely III RR, Nevzorov AV, Ritter C, Sakai T, Santer BD, Sato M, Schmidt A, Uchino O, Vernier JP (2014) Total volcanic stratospheric aerosol optical depths and implications for global climate change. Geophys Res Lett 41:7763–7769

Senghor H, Machu É, Hourdin F, Gaye AT (2017) Seasonal cycle of desert aerosols in western Africa: analysis of the coastal transition with passive and active sensors. Atmos Chem Phys 17:8395–8410

Smith RL (1968) Upwelling. Oceanogr Mar Biol Annu Rev 6:11–46

Stein AF, Draxler RR, Rolph GD, Stunder BJ, Cohen MD, Ngan F (2015) NOAA's HYSPLIT atmospheric transport and dispersion modeling system. Bull Am Meteorol Soc 96:2059–2077

Van der Does M, Korte LF, Munday C, Brummer I, Geert-Jan A, Stuut J-B (2016) Modal grain-sizes of Saharan dust in the Atlantic Ocean measured in 7 sediment traps from 2012 to 2013. Pangaea. https://doi.org/10.1594/pangaea.863052

Vernier J-P, Thomason LW, Pommereau J-P, Bourassa A, Pelon J, Garnier A, Hauchecorne A, Blanot L, Trepte C, Degenstein D, Vargas F (2011) Major influence of tropical volcanic eruptions on the stratospheric aerosol layer during the last decade. Geophys Res Lett 38:L12807. https://doi.org/10.1029/2011GL047563

Vimont DJ, Kossin JP (2007) The Atlantic meridional mode and hurricane activity. Geophys Res Lett 34:L07709. https://doi.org/10.1029/2007GL029683

Washington R, Todd MC (2005) Atmospheric controls on mineral dust emission from the Bodélé depression, Chad: the role of the low level jet. Geophys Res Lett 32:L17701. https://doi.org/10.1029/2005GL023597

Wong S, Dessler AE, Mahowald MN, Yang P, Feng Q (2009) Maintenance of lower tropospheric temperature inversion in the Saharan air layer by dust and dry anomaly. J Clim 22:5149–5162

Zuluaga MD, Webster PJ, Hoyos CD (2012) Variability of aerosols in the tropical Atlantic Ocean relative to African easterly waves and their relationship with atmospheric and oceanic environments. J Geophys Res 117:D16207. https://doi.org/10.1029/2011JD017181